IEEE Access
Multidisciplinary | Rapid Review | Open Access Journal

Received July 6, 2021, accepted July 19, 2021, date of publication July 26, 2021, date of current version August 3, 2021.

Digital Object Identifier 10.1109/ACCESS.2021.3099760

Electric and Magnetic Field Estimation Under Overhead Transmission Lines Using Artificial Neural Networks

AJDIN ALIHODZIC, (Member, IEEE), ADNAN MUJEZINOVIC, (Member, IEEE), AND EMIR TURAJLIC, (Member, IEEE)
Faculty of Electrical Engineering, University of Sarajevo, 71000 Sarajevo, Bosnia and Herzegovina
Corresponding author: Ajdin Alihodzic (ajdin.alihodzic@etf.unsa.ba)

ABSTRACT In this paper, a novel method for electric field intensity and magnetic flux density estimation in the vicinity of the high voltage overhead transmission lines is proposed. The proposed method is based on two fully connected feed-forward neural networks to independently estimate electric field intensity and magnetic flux density. The artificial neural networks are trained using the scaled conjugate gradient algorithm. Training datasets corresponds to different overhead transmission line configurations that are generated using an algorithm that is especially developed for this purpose. The target values for the electric field intensity and magnetic flux density datasets are calculated using the charge simulation method and Biot-Savart law based method, respectively. This data is generated for fixed applied voltage and current intensity values. In instances when the applied voltage and current intensity values differ from those used in the artificial neural network training, the electric field intensity and magnetic flux density results are appropriately scaled. In order to verify the validity of the proposed method, a comparative analysis of the proposed method with the charge simulation method for electric field intensity calculation and Biot-Savart law-based method for magnetic flux density calculation is presented. Furthermore, the results of the proposed method are compared to measurement results obtained in the vicinity of two 400 kV transmission lines. The performance analysis results showed that proposed method can produce accurate electric field intensity and magnetic flux density estimation results for different overhead transmission line configurations.

INDEX TERMS Artificial neural networks (ANN), Biot-Savart (BS) law based method, charge simulation method (CSM), electric field intensity, magnetic flux density, scaled conjugated gradient (SCG).

I. INTRODUCTION

Numerous epidemiological studies were conducted trying to find correlation between exposure to magnetic and electric fields, and human diseases. Analysis of data collected from several studies on the influence of low frequency magnetic field on the development of childhood leukemia showed that the existence of a small but not negligible risk of leukemia associated with exposure to fields above 0.3 μT [1]. Studies conducted in the United States and France, which analysed data on cases of childhood leukemia, after 1988 found that the proximity of the place of residence to 200+ kV transmission lines could be associated with a small increase in the risk of childhood leukemia [1]–[3].

Although the International Agency for Research on Cancer has classified low-frequency magnetic fields as a potential cause of cancer, due to the observed association between field exposure and the development of childhood leukemia, not all effects of exposure on human health have been fully understood [4]. In order to limit the impact of electric and magnetic fields on the environment, many international and national institutions have defined limit values for fields that can occur in different areas. Although epidemiological studies have established a statistical association between exposure to electric and magnetic fields and the development of severe diseases in humans, the main objective of these generally accepted limit values is to prevent the occurrence of induced currents that approach the values of currents that might produce neuron excitation [5].

As a result of exposure to strong electric fields, values above 5 kV/m, the induced currents can occur in the human body, as well as stimulation of nerves and muscles [6].

The International Commission on Non-Ionizing Radiation Protection [7], based on the hitherto known effects

The associate editor coordinating the review of this manuscript and approving it for publication was Shuihua Wang.

This work is licensed under a Creative Commons Attribution 4.0 License. For more information, see https://creativecommons.org/licenses/by/4.0/

of low-frequency electric and magnetic fields, published in 2010 guidelines for limiting exposure to time-varying electric and magnetic fields (1 Hz - 100 kHz). According to these guidelines the reference levels are 10 kV/m and 1 mT for occupational exposure to 50 Hz electric and magnetic fields and 5 kV/m and 0.2 mT for general public exposure.

Although extremely low frequency electric and magnetic fields act and support each other at the same time, due to the negligible value of the displacement current intensity, it is a common practice to measure and calculate these fields separately [8]. The purpose of measuring and calculating electric and magnetic fields near the elements of the power system is to detect locations where their values exceed the allowed field values.

The daily increase in the electricity requirements and environmental constraints that are set when building new transmission lines, require constant effort on finding the optimal design to maximize power transmission without violating the set of limits in terms of capacity, safety distances, maximum allowable electric and magnetic fields, noise levels, etc. Therefore, when planning the construction of new transmission lines and choosing the configuration of the conductors, it is important to correctly calculate the maximum level of electric and magnetic fields that may occur in their environment, in order to meet the prescribed values [7], [9]–[11].

It is well known fact that electric field intensity is a function of applied voltage, while the magnetic field is a function of current intensity. The distribution of these fields in the vicinity of transmission lines also depends on the arrangement of conductors, the height of phase conductors, the order of phase conductors the shape of the ground. When choosing the routes of transmission lines, it is desirable to avoid populated areas, but this is often not possible. Alternatively, in populated areas the overhead transmission lines could be replaced by underground cables, but this solution complicates and significantly increases the project cost [12].

Over the past decades, various measurement and calculation methods have been developed to determine the electric field intensity and magnetic fields in the vicinity of power facilities such as overhead transmission lines and substations (SS). The calculation methods can be further categorized as analytical and numerical methods.

Due to the complexity of the model, the calculation of the magnetic field by direct application of Maxwell's equations is only possible for simple configurations [13]. The advantage of analytical models is their ability to express the dependence of the field intensity on the transmission line parameters, and simpler for analyzing new configurations. The disadvantage of such models is that they are based on numerous assumptions [14].

For analytical calculation of electric and magnetic fields the multi pole expansion can be used [15], [16], and also the procedure based on a discrete approximation of the Biot-Savart law for magnetic fields [17]. For numerical calculations of electromagnetic fields near power lines, the following methods are used, among others: finite-difference method (FDM), finite element method (FEM), boundary element method (BEM), charge simulation method (CSM), surface charge simulation method (SCSM) [18]. Heuristic algorithms have been used in conjunction with some of the previously mentioned calculation methods in order to optimize certain parameters that are part of the electric and magnetic field calculations in the vicinity of the transmission lines [19], [20]. Most commonly, heuristic algorithms are applied to optimize the number and positions of simulating charges in CSM method. Heuristic algorithms are also applied to the transmission line geometry optimization problem [12].

In addition, different artificial neural network (ANN) models have been used for electric field intensity and magnetic flux density estimation. These include general regression neural networks [21], multilayer perceptron [22], normalized radial basis function networks [14].

In this paper, a novel method for electric field intensity and magnetic flux density estimation under overhead transmission lines is proposed. The principal advantage of the proposed methodology is that it is able to produce accurate electric field intensity and magnetic flux density estimates in the vicinity of overhead transmission lines for a different overhead transmission line configurations and for a range of different applied voltages and currents.

The rest of the paper is organized as follow. Section 2 describes the proposed method. Section 3 presents the validation of proposed method, where the results of a comparative analysis of the proposed method with charge simulation method and Biot-Savart law based method are presented. In, addition the performance of the proposed method is evaluated by comparing with electric field intensity and magnetic flux density measurement data. Section 4 concludes the paper.

II. PROPOSED METHOD FOR ELECTRIC AND MAGNETIC FIELD ESTIMATION

A. ARTIFICIAL NEURAL NETWORKS

Artificial neural networks, consisting of simple processing units (neurons), are massively parallel distributed processors which have an inherent predisposition for learning, generalization and storing experiential knowledge [23]–[26]. In this paper, two fully connected feed-forward ANNs are designed to independently estimate electric field intensity and magnetic flux density. These two ANNs are trained to estimate the electric field intensity and magnetic flux density for a range of different transmission line conductor configurations.

The data collection and preparation, network architecture and the choice of learning algorithm are important elements in the process of an ANN model development.

First, the ANN model for electric field intensity estimation is considered. Here, each training sample that is used to describe a particular transmission line geometry is defined by 9 coordinate values. Here, each sample in the training dataset describes a particular overhead transmission line configuration. Each considered overhead transmission line configuration consists of 5 conductors: 3 phase conductors and

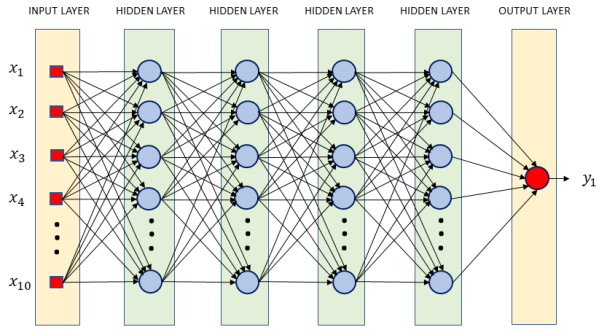

FIGURE 1. Artificial neural network model for electric/magnetic field estimation.

2 shielding wires. Thus, the geometrical description of overhead transmission line entails 5 (x,y) points in two dimensional space. However, the coordinate system is defined so that the horizontal coordinate of the central phase conductor is equal to zero. Therefore, it is sufficient to use 9 coordinate values to completely define the geometry of an overhead transmission line. In addition, every sample in the training dataset contains the lateral distance of the point of electric field intensity estimation from the central phase conductor (central vertical line). Thus, the ANN inputs layer consists of 10 inputs. The neural network output is an estimate of the electric field intensity for given power line conductor geometry at a point 1 m above the ground surface and some lateral distance away from the central vertical line. Thus, the output layer contains only 1 artificial neuron. For each training sample the target value (desired neural network output) is electric field intensity. This value is obtained using CSM. Each sample in the training dataset is defined by a 10-dimensional input vector and a corresponding desired target value (scalar).

Similarly, a separate ANN is used to estimate the magnetic flux density in vicinity of overhead transmission lines. The target values for the magnetic flux density dataset are calculated using BS law based method. Both ANNs are specified and trained in a similar manner. The ANNs use the same network architecture, as shown in Fig. 1.

Both models are fully connected feed-forward artificial neural networks consisting of one input layer, 4 hidden layers and 1 output layer. The input layer has 10 inputs and the output layer has 1 output. Each hidden layer has 20 neurons. The proposed neural network architecture has a sufficient number of free parameters to describe some very complex input-output relations, including the relationships between the various overhead transmission line configurations and electric field intensity/magnetic flux density values at points lying within a considered range of lateral displacement from the central vertical line and at a height of 1 m above the ground surface.

For the purpose of ANN training, 200,000 different overhead transmission line configurations are considered. These configurations are generated using an algorithm that is especially developed for this purpose. Two datasets of same size are generated. One dataset is used to train the ANN model for electric field intensity estimation and the other dataset is used to train the second ANN model for magnetic flux density estimation. For each overhead transmission line configuration, the target electric field intensity and magnetic flux density values are generated for 81 points with different lateral displacement from the central vertical line. The considered points are found from -40 m to 40 m away from the central vertical line at 1 m above the ground surface. Thus, each dataset consists of 16,200,000 samples. The two datasets only differ in terms of target values. The target values for the electric field intensity dataset are calculated using CSM under the assumption that phase-to-phase voltage of 400 kV is applied. The target values for the magnetic flux density dataset are evaluated using BS based law method under the assumption that 100 A current intensity flows through phase conductors and that overhead transmission line is symmetrically loaded. A detail description of training data generation process is described in the section that follows. Prior to training, the data is randomly selected to form the training (70% samples), validation (15% samples), and test (15% samples) datasets.

The ANNs are trained under the supervised learning paradigm. The scaled conjugate gradient (SCG) algorithm [27] is used to train both neural network models. SCG algorithm belongs to a larger category of conjugate gradient methods. Generally, the conjugate gradient algorithms have low memory requirements and are also attributed with strong global and local convergence characteristics [28]. Scaled conjugate gradient algorithm uses the second-order information and thus, its convergence speed increases as it approaches the cost function minimum [27]. The conjugate gradient algorithm defines the iterative procedure to update the synaptic weights [27]:

$$w_{k+1} = w_k + \alpha_k \cdot p_k \tag{1}$$

where k denotes the current iteration, usually called epoch, and α_k denotes the learning rate. The term p_k denotes the search direction and its update is defined as:

$$p_{k+1} = -E'(w_{k+1}) + \beta_k \cdot p_k \tag{2}$$

Its initial value corresponds to $p_0 = -E'(w_0)$. Here, $E'(w_k)$ describes the cost (error) function that depends on the weights and biases of the network. The error function gradient at with respect to weights w_k is denoted as $E'(w_k)$. Various versions of the conjugate gradient algorithm [29], [30] propose different ways of evaluating the factor β_k. Most conjugate gradient methods adapt the learning rate α_k at each iteration. The update of learning rate value aims to minimize the error function along the search direction. Commonly, conjugate gradient algorithms use a line search technique to evaluate the optimal learning rate (step size) value. The SCG algorithm was developed in order to avoid the time-consuming line search [27]. The scaled conjugate gradient method uses the

Levenberg-Marquardt approach to scale the step size [27]:

$$s_k = \frac{E'(w_k + \sigma_k \cdot p_k) - E'(w_k)}{\sigma_k} + \lambda_k \cdot p_k \tag{3}$$

Here σ_k and λ_k denote the scaling factors that are used in the approximation of the Hessian matrix. This step size scaling mechanism decreases the number of computations performed in each iteration compared to the line search method. SCG performance is not significantly affected by any user-dependent parameters and for networks with a large number of free weights, the scaled conjugate gradient algorithm is shown to be particularly efficient [27].

B. GEOMETRY GENERATION

The ANN training dataset is generated using different overhead transmission line configurations. Each configuration of overhead transmission line is defined using a two-stage procedure. In the first stage, the phase conductor positions are generated, while in the second stage, the number and the positions of the shielding wires is determined. As a reference case, overhead transmission line rated voltage is 400 kV, phase current intensity is 100 A, and each phase conductor is composed of two sub-conductors in the bundle. The radius of each bundle is 20 cm and radius of used the sub-conductor is 1.521 cm.

1) PHASE CONDUCTOR POSITION

Different overhead transmission line configurations are categorized into one of five distinct configuration types. The phase conductor positions are randomly selected within the constrains that define a given configuration type. In each case, the minimum height of the phase conductor was set to $y_{min} = 6.44$ m and minimal distance between two adjacent phase conductors is $d_{min} = 7.4$ m. Furthermore, in each configuration type, x coordinate value of the bundle center of the central phase conductor along the x-axis is set to zero, $x_1 = 0$. The x coordinate values of the bundle center of the remaining two phase conductors, x_2 and x_3, are defined in terms of their distance from x_1. The graphic illustration of the generated transmission line configurations is shown in Fig. 2.

Horizontal configuration of phase conductors is shown in Fig. 2a. All phase conductors have identical heights, $y_1 = y_2 = y_3$. Their height can take values in a range from y_{min} to $y_{min} + \Delta y$, where Δy is a randomly selected number in the range [0 - 13.56]. The outer phase conductors are equidistant from the central conductor $x_2 = -x_3$. The distance between the outer and the central phase conductors is constrained within a range d_{min} to $d_{min} + \Delta x$, where Δx is randomly generated number in the range of [0 - 7.6].

Vertical configuration of the phase conductors is shown in Fig. 2b. Here, all phase conductors are placed along the coordinate system ordinate. Thus, $x_1 = x_2 = x_3 = 0$. In this transmission line configuration type the height of the lowest phase conductor, y_1, is constrained to within a range from y_{min} to $y_{min} + \Delta y$, where Δy is randomly generated number within the range of values [0 - 2]. In this configuration, the neighboring phase conductors are equidistant. The vertical distance between two adjacent phase conductors is constrained to within the range of d_{min} to $d_{min} + \Delta y_1$, where Δy_1 is in the range [0 - 2].

Fig. 2c shows a configuration type where the height of the outer phase conductors differs from the height of the central conductor. In this case, the outer phase conductors have equal heights. The height of the central phase conductor, y_1, is constrained to within a range from y_{min} to $y_{min} + \Delta y$, where Δy is randomly selected number in the range [0 - 13.56]. The height of the outer phase conductors is defined by the following equation $y_2 = y_3 = y_{min} + \Delta y_1$, where Δy_1 is randomly generated number in the range [0 - 13.56]. The outer phase conductors are equidistant from the central phase conductor along the x-axis, $x_2 = -x_3$. The x coordinate values of outer phase conductors are defined by the following equation:

$$x_2 = -x_3 = d_{min} \cdot \cos\alpha + \Delta x \tag{4}$$

where α denotes the angle defined in Fig. 2c and Δx is a randomly generated number. The maximum displacement of outer phase conductors from the central phase conductor along the x-axis is constrained to 15 m.

In Fig. 2d, another configuration type is shown. Here the outer phase conductors are equidistant from the central conductor along x-axis, $x_2 = -x_3$, while the heights of all phase conductors are different $y_1 \neq y_2 \neq y_3$. The heights of the phase conductors are in the range from y_{min} to $y_{min} + \Delta y_i$, where Δy_i is a randomly generated number within the range [0 - 13.56] for the i-th phase conductor, $i = 1,2,3$. On the other hand, the x coordinate values of the outer phase conductors are defined as:

$$x_2 = -x_3 = d_{min} \cdot \cos\alpha_2 + \Delta x_2 \tag{5}$$

where α_2 is the angle defined in Fig. 2d and Δx is a random generated number. The maximum distance of the outer phase conductor from the central phase conductor is limited to $\pm$ 15 m.

The final configuration type is shown in Fig. 2e. With the exception of $x_1 = 0$, the coordinate values of the phase conductors are randomly selected within the range - 15 m $< x_j <$ 15 m, $j = 2, 3$ and $y_{min} < y_i < 20$ m, $i = 1, 2, 3$. As previously stated, the first phase conductor is placed along the ordinate of coordinate system while the other two phase conductors have randomly generated positions within the defined range. The coordinates of phase conductors are generated in such a way that the minimum distance between phase conductors is equal or greater than d_{min}.

2) SHIELDING WIRES POSITION

When calculating electric field intensity, the number and the position of shielding wires significantly affect the electric field intensity distribution. On the other hand, when current in system is symmetric, the shielding wires does not significantly affect the distribution of magnetic flux density [31], [32] i.e. the impact of the shielding wire(s) is negligible.

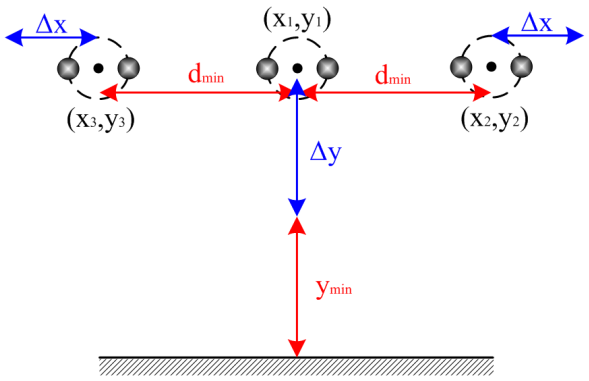

(a) Horizontal configuration

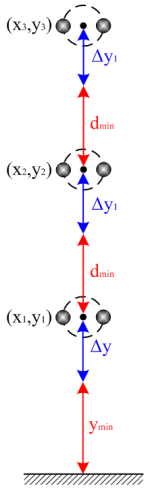

(b) Vertical configuration

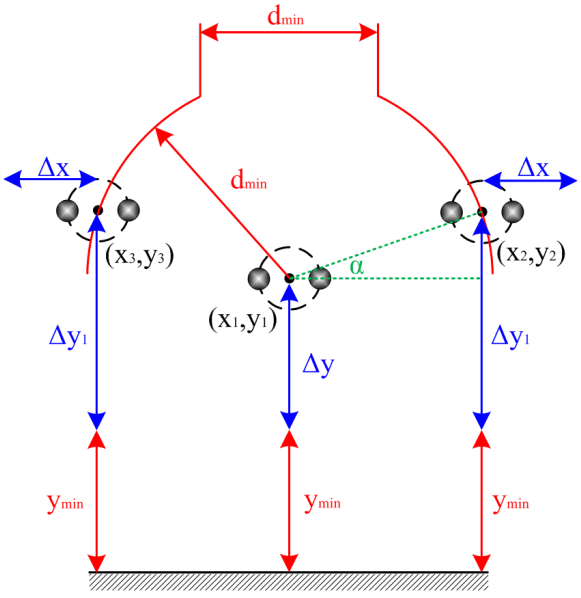

(c) Configuration with same height of outer conductors

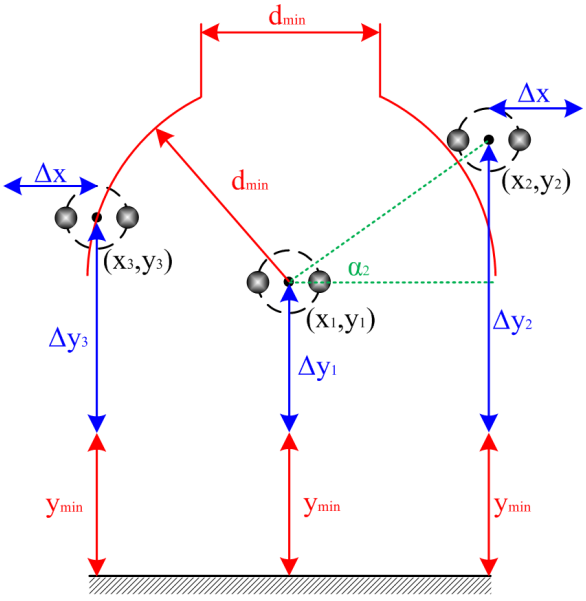

(d) Configuration with different height of phase conductors

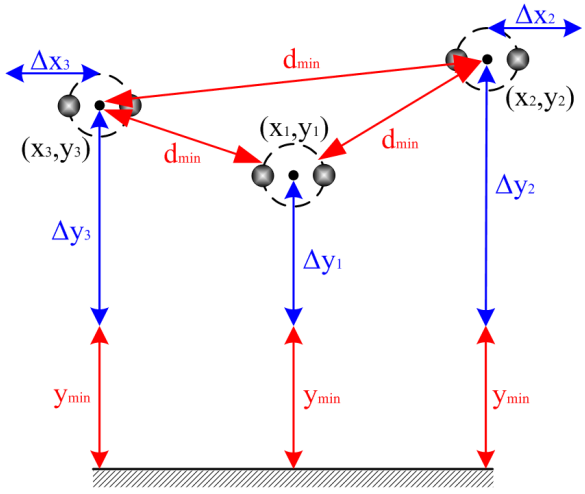

(e) Configuration with different heights and distances between phase conductors

FIGURE 2. Generated overhead transmission line configurations.

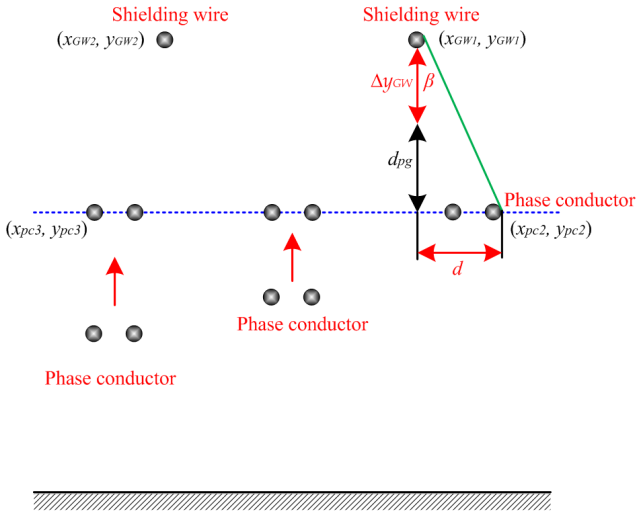

FIGURE 3. Positioning of the shielding wires.

In order to simplify the problem of determining the position and number of shielding wires, it is assumed that the heights of all phase conductors are equal to each other and equal to the height of the highest phase conductor of the considered configuration, as shown in Fig. 3. The x and y coordinate of first shielding wire is determined by using following equations:

$$x_{GW1} = \frac{x_1 + x_2 + x_3}{3} \tag{6}$$

$$y_{GW1} = \Delta y_{GW1} + (d_{pg} + y_{pc}) \tag{7}$$

where Δy_{GW1} is a randomly generated number within the range [0 - 3], $d_{pg} = 6{,}44$ m is minimal vertical distance between shielding wire and phase conductors and y_{pc} is the height of phase conductors.

The efficiency check of shielding wire is done by comparing distance d and longitudinal distance between the shielding wire and the outer phase conductor. The distance d is calculated by using the following equation:

$$d = (y_{GW1} - y_{pc}) \cdot \tan\beta \tag{8}$$

where β is the shielding angle [33]. Within the model shielding angle with maximum value of 20° was assumed to provide sufficient protection level.

If the longitudinal distance between the shielding wire and the outer phase conductor is lower or equal to the distance d it was assumed that one shielding wire is sufficient, and therefore, the second shielding wire is considered unnecessary. Since the number of ANN inputs is fixed, a second shielding wire must be given some coordinate values. The lack of second shielding wire can be effectively represented by placing the second shielding wire at infinity height. In this model the height was set to 10^{15} m. Due to the huge height, second shielding wire does not affect the calculation results of electric field intensity. When one shielding wire does not give the satisfactory protection level, i.e. the longitudinal distance between the shielding wire and the foremost point of the outer phase conductor is higher than distance d, the second shielding wire is required.

When two shielding wires are used, both shielding wires are set to the same height, as determined by equation (7). The x coordinates of the shielding wires are determined in relation to the outer phase conductors by using the following equations:

$$x_{GW1} = x_{pc2} - d \tag{9}$$

$$x_{GW2} = x_{pc3} + d \tag{10}$$

C. ELECTRIC FIELD INTENSITY AND MAGNETIC FLUX DENSITY CALCULATION

The target values for each sample in the ANN training dataset for electric field intensity estimation are calculated using the CSM method. On the other hand, the target values for the ANN based model for estimation of magnetic flux density are generated according to a BS law based method. For both, electric field intensity and magnetic flux density calculations, the 2D algorithms have been used.

1) ELECTRIC FIELD INTENSITY CALCULATION METHOD

Charge simulation method has been used to calculate the electric field intensity in the proximity of the overhead transmission lines. According to this method, the source of the electric field are fictitious point charges. Each phase conductor and each shielding wire of the overhead transmission line can be treated as one fictitious point charge. Since the reference case uses bundle conductors composed of two sub-conductors, it is possible to determine the radius of an equivalent conductor. The radius of the equivalent conductor is defined by the following equation [34]:

$$r_{ec} = R \cdot \sqrt[N]{\frac{N \cdot r_{sc}}{R}} \tag{11}$$

where r_{ec} is the radius of the equivalent conductor, N is number of the sub-conductors in the bundle, r_{sc} is the radius of sub-conductors and R is the radius of the bundle. The radius of the bundle is calculated by following equation [35]:

$$R = \frac{B}{\left[2 \cdot \sin\frac{\pi}{N}\right]} \tag{12}$$

where B is the spacing between the adjacent sub-conductors.

The used CSM method consists off two steps:

- calculation of the phasors of the fictitious point charges,
- calculation of the vector components of electric field intensity phasor caused by fictitious point charges.

In the 2D CSM algorithm, the phasors of the fictitious point charges are calculated using the following matrix equation:

$$\{\underline{\varphi}\} = [P] \cdot \{\underline{q}\} \tag{13}$$

where $\{\underline{\varphi}\}$ is a matrix of electric potential phasors, $\{\underline{q}\}$ is a matrix of the unknown point charge phasors and $[P]$ is a square matrix of potential coefficients. Each overhead transmission line conductor is represented by one fictitious point charge. Thus, in the case of phase conductor, elements of the matrix of electric potential phasors are equal to line-to-ground voltage phasor, while in the case of shielding wire,

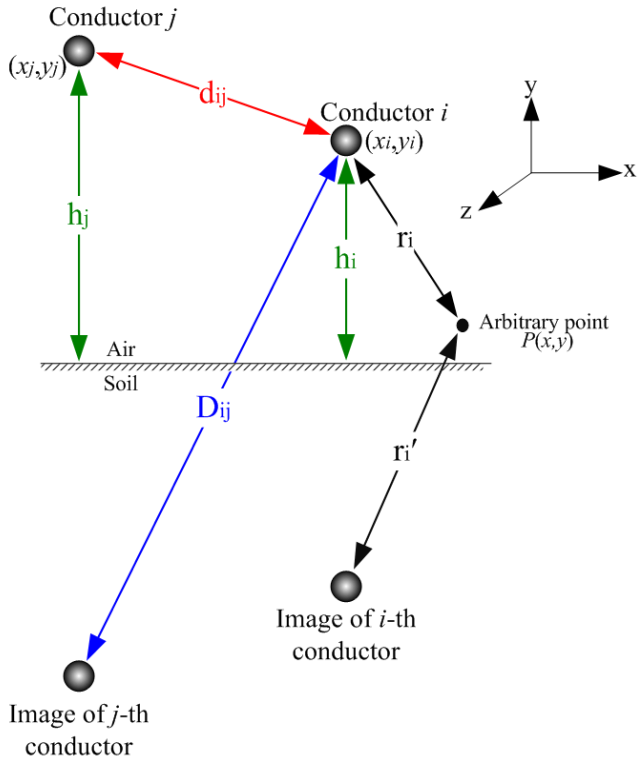

FIGURE 4. The distances between the point charges, the image of point charges and an arbitrary point [34].

they are equal to zero. Potential coefficients of the matrix [P] are calculated using the following equations [34]:

$$P_{ii} = \frac{1}{2\pi \cdot \varepsilon_0} \cdot \ln \frac{2 \cdot y_i}{r_{eci}} \tag{14}$$

$$P_{ij} = \frac{1}{2\pi \cdot \varepsilon_0} \cdot \ln \frac{D_{ij}}{d_{ij}} \tag{15}$$

where ε_0 denotes the dielectric constant of air, y_i is y coordinate of the i-th equivalent conductor, r_{eci} is the radius of the i-th equivalent conductor, d_{ij} is the shortest distance between i-th and j-th conductor and D_{ij} is the shortest distance between i-th conductor and the image of j-th conductor. All relevant parameters of the analysed system are shown in Fig. 4.

When calculating the electric field intensity in the proximity of the overhead transmission lines, the impact of the ground surface must be taken into consideration. Complex image method, is used to take into account the impact of the ground surface. This further implies that the influence of the soil surface can be taken into account by reflecting the point fictitious charge below the soil surface at a depth equal to the product of the height of the conductor above the surface and the complex coefficient $\underline{\Gamma}$ [18], [36]. Complex coefficient $\underline{\Gamma}$ is defined by the following equation:

$$\underline{\Gamma} = \frac{j \cdot \omega \cdot \varepsilon_0 - (\sigma + j \cdot \omega \cdot \varepsilon_{soil})}{j \cdot \omega \cdot \varepsilon_0 + (\sigma + j \cdot \omega \cdot \varepsilon_{soil})} \approx -1 \tag{16}$$

where ω is power system angular frequency, σ is soil conductivity, ε_{soil} is dielectric permittivity of the soil. For all practical cases, complex coefficient $\underline{\Gamma}$ is approximately equal -1.

By solving the matrix equation (13), the phasors of fictitious point charges are determined, which is a prerequisite for determining the components of the electric field intensity phasor at points of interest. Subsequently, the vector components of the electric field intensity phasor at some arbitrary point $P(x, y)$, is determined using the following equations:

$$\underline{E}_x(x, y) = \sum_{i=1}^{n} \frac{\underline{q_i}}{2\pi \cdot \varepsilon_0} \cdot \left(\frac{x - x_i}{r_i^2} + \underline{\Gamma} \frac{x - x_i}{r_i'^2} \right) \tag{17}$$

$$\underline{E}_y(x, y) = \sum_{i=1}^{n} \frac{\underline{q_i}}{2\pi \cdot \varepsilon_0} \cdot \left(\frac{y - y_i}{r_i^2} + \underline{\Gamma} \frac{y + y_i}{r_i'^2} \right) \tag{18}$$

where $\underline{E}_x(x, y)$ and $\underline{E}_y(x, y)$ are x and y vector components of the electric field intensity phasor at an arbitrary point (x,y), $\underline{q_i}$ is phasor of i-th fictitious point charge, (x,y) are coordinates of an arbitrary point, (x_i,y_i) are coordinates of the i-th fictitious point charge, r_i is the shortest distance between the i-th fictitious point charge and the arbitrary point, r_i' is the shortest distance between complex image of the i-th fictitious point charge and the arbitrary point and n is the total number of fictitious point charges in the system.

Based on the values determined by equations (17) and (18), the resultant value of the electric field intensity at some arbitrary point is defined as:

$$E(x, y) = \sqrt{\left|\underline{E}_x(x, y)\right|^2 + \left|\underline{E}_y(x, y)\right|^2} \tag{19}$$

where $E(x, y)$ is the resultant value of the electric field intensity in arbitrary point with coordinates (x, y).

2) MAGNETIC FLUX DENSITY CALCULATION METHOD

For each generated configuration, the magnetic flux density phasor is calculated by using the method based on Biot-Savart law. According to this method, source of the magnetic field are point current sources which are located at the center of each equivalent conductor. Under the previously stated assumption, the vector components of the magnetic flux density phasor at an arbitrary point $P(x, y)$ can be calculated using the following equations [37]:

$$\underline{B}_x(x, y) = \frac{\mu_0}{2\pi} \cdot \sum_{i=1}^{n} \left(-\frac{y - y_i}{r_i^2} + \frac{y + y_i + \alpha}{r_i'^2} \right) \cdot \underline{I}_i \tag{20}$$

$$\underline{B}_y(x, y) = \frac{\mu_0}{2\pi} \cdot \sum_{i=1}^{n} \left(\frac{x - x_i}{r_i^2} - \frac{x - x_i}{r_i'^2} \right) \cdot \underline{I}_i \tag{21}$$

where $\underline{B}_x(x, y)$ and $\underline{B}_y(x, y)$ are x and y vector components of the magnetic flux density phasor at point (x,y), μ_0 is magnetic permeability of air, n is the total number of current point sources, $\underline{I}_i$ is current intensity phasor of i-th point source, (x,y) are coordinates of an arbitrary point, (x_i,y_i) are coordinates of the i-th current point source, $\underline{\alpha}$ is the complex depth, r_i is the shortest distance between the i-th current point source and arbitrary point, r_i' is the shortest distance between complex image of i-th current point source and arbitrary point and n is total number of current point sources in the system. All relevant geometric parameters are presented in Fig. 5.

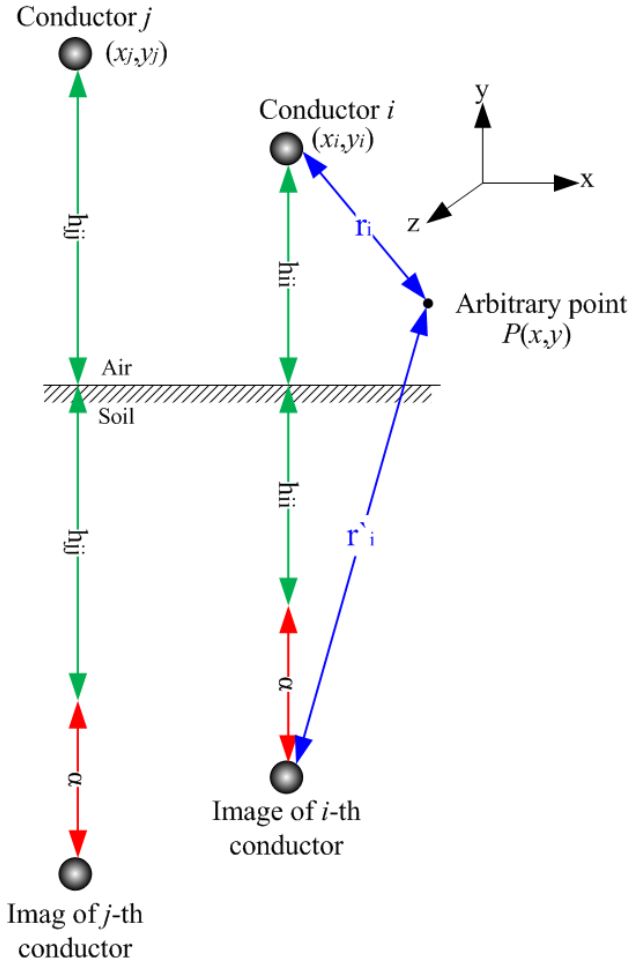

FIGURE 5. The distance between the current point source, the image of current point source and an arbitrary point.

In the equations (20) and (21), the effect of ground surface is taken into account by using the complex image method. According to this method, the image of the current point sources is placed at a depth below the ground surface equal to the distance of point current sources above the ground surface but increased by the complex distance $\underline{\alpha}$, as showed in Fig. 5. The complex distance $\underline{\alpha}$ is defined by the following equation [38]:

$$\underline{\alpha} = \frac{2}{\sqrt{-j \cdot \omega \cdot \mu_0 \cdot (\sigma_{soil} - j \cdot \omega \cdot \varepsilon_{soil})}} \tag{22}$$

Since 2D calculation algorithm is used, third component of the magnetic flux density vector was neglected i.e. $\underline{B}_z = 0$.

Finally, the resultant value of the magnetic flux density at some arbitrary point is defined as:

$$B(x, y) = \sqrt{\left|\underline{B}_x(x, y)\right|^2 + \left|\underline{B}_y(x, y)\right|^2} \tag{23}$$

where $B(x, y)$ is the resultant value of the magnetic flux density at an arbitrary point with coordinates (x, y).

D. CONSIDERATION OF VOLTAGE AND CURRENT VARIATIONS

In literature, it is a common approach to calculate the electric field intensity using the rated transmission line voltage [39], [40]. For the 400 kV network, which is used as the reference case, Grid Code [41] and IEC 60038 [42] allow deviations of applied voltage values from rated voltage in range from $-$ 10% to $+$ 5%. However, in South East Europe 400 kV network even higher long term voltage deviations are registered [43]. Therefore, for accurate estimation of electric field intensity, true value of applied voltage needs to be taken into account. In Fig. 6a hourly voltage values are given for the one year period (from 1st January to 31st December 2020) measured in 400 kV SS Sarajevo 10. It can be noted that the voltage value vary over the time. In Fig. 6b voltage duration curve is given for the analysed period. More than 90% of time voltage value is higher than the maximum allowable value according to the Grid Code and IEC 60038, and 99% of time is higher than the rated network voltage. These increased voltage values are caused by the underloaded transmission lines and domestic reactive energy production as well as injected by interconnection lines from neighboring systems [43].

Furthermore, in literature, some authors use overhead transmission line rated current intensity as input parameter to calculate magnetic flux density, in order to estimate worst case magnetic flux density [44]. It is a well known fact that the overhead transmission line current intensity varies over the time with load. In Fig. 7a variation of the current intensity of transmission line SS Sarajevo 10 - SS Sarajevo 20 is shown.

From diagram given in Fig. 7a it is noticeable that current also significantly vary over the time. In Fig. 7b the duration in % of time of current intensity is given. From this figure, it is noticeable that the current intensity of the analysed transmission line over the entire analysed period (year 2020) is much lower than the transmission line ampacity. For that this transmission line, the ampacity is approximately 1900 A [44].

The proposed model is able the estimate accurate electric field intensity and magnetic flux density values not only for the different transmission line typologies, but also for any range of applied voltages and current intensities. The ANNs are trained to estimate the electric field intensity and magnetic flux density for the fixed values of applied voltage and current intensity values (400 kV and 100 A). When transmission line currents and voltages differ from those used to train the neural networks, it is necessary to perform adequate scaling of the ANN outputs in order to obtain appropriate values.

Electric field intensity and magnetic flux density scaling is performed by the following equations:

$$E_n = \frac{U_n}{U_s} \cdot E_s \tag{24}$$

$$B_n = \frac{I_n}{I_s} \cdot B_s \tag{25}$$

where U_n is the actual applied voltage, U_s is the applied voltage used for training ANN, I_n is the actual current intensity, I_s is the current intensity used for training ANN, E_s is the

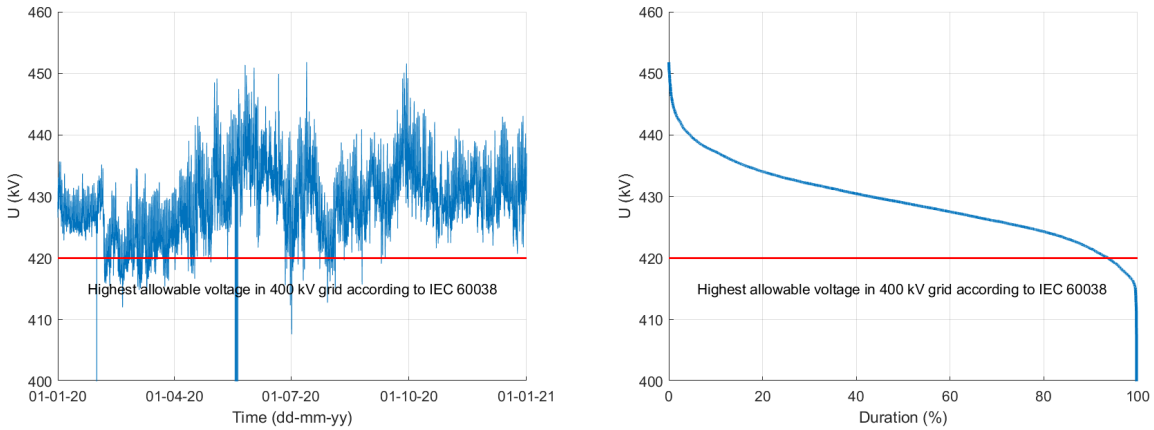

(a) Diagram of voltage variation

(b) Voltage duration curve

FIGURE 6. Voltage on 400 kV SS Sarajevo 10 in 2020.

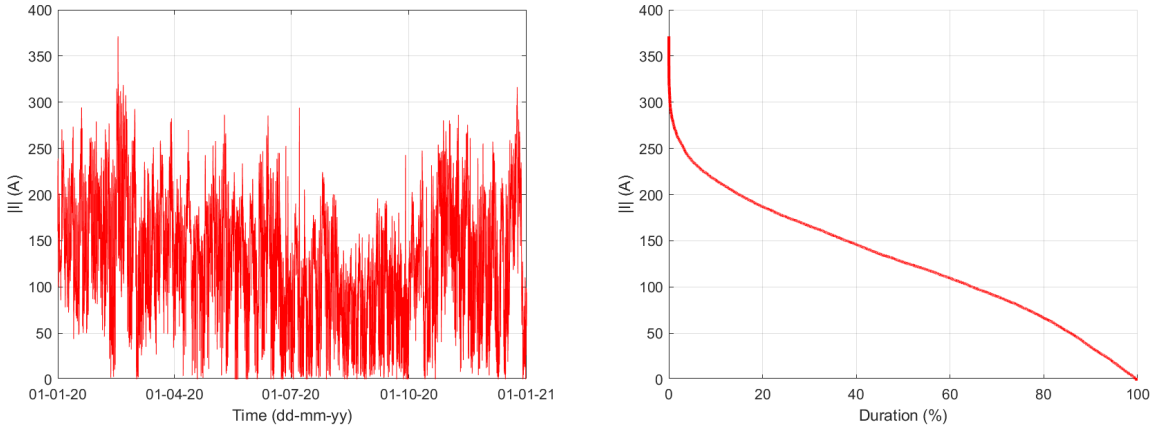

(a) Diagram of current intensity variation

(b) Current intensity duration curve

FIGURE 7. Current intensity on 400 kV overhead transmission line SS Sarajevo 10 - Sarajevo 20 in 2020.

electric field intensity obtained by ANN, B_s is the magnetic flux density obtained by ANN, E_n is the scaled electric field intensity and B_n is the scaled magnetic flux density.

III. VALIDATION OF PROPOSED METHOD

Validation of the proposed method for the estimation of the electric field intensity and magnetic flux density was done by comparing results with the calculations obtained by charge simulation method and method based on Biot-Savart law, respectively. In addition the performance of the proposed method is also evaluated using the measurement results. The comparative analysis is based on different overhead transmission line configurations.

A. COMPARISON WITH CALCULATION RESULTS

The comparative analysis of the proposed method with CSM and BS law based method is conducted for three different overhead transmission line configurations, as shown in Fig. 8. First analysed case is an overhead transmission line of horizontal configuration of phase conductors with two shielding wires, as showed in Fig. 8a [44]. Second analysed case is an overhead transmission line of vertical phase conductors configuration with a single shielding wire, as showed in Fig. 8b. Third analysed configuration in this section is a delta phase conductor configuration with two shielding wires, as showed in Fig. 8c. For each configuration, the associated geometric parameters are shown.

The proposed method for the electric field intensity estimation is evaluated for three different applied voltage values, 400 kV, 440 kV and 360 kV. On the other hand, the magnetic flux density is calculated for two different current intensity values 100 A and 1000 A. Both, the electric field intensity and the magnetic flux density values, are calculated 1 m above ground surface and for the lateral profile in the range from -40 m to 40 m, with increments of 1 m.

Fig. 9 show the electric field intensity calculation results by CSM and the proposed method for the horizontal configuration of overhead transmission line. Three different applied voltage levels are considered. Similarly, in Fig. 10 the results of magnetic flux density calculations by BS based law

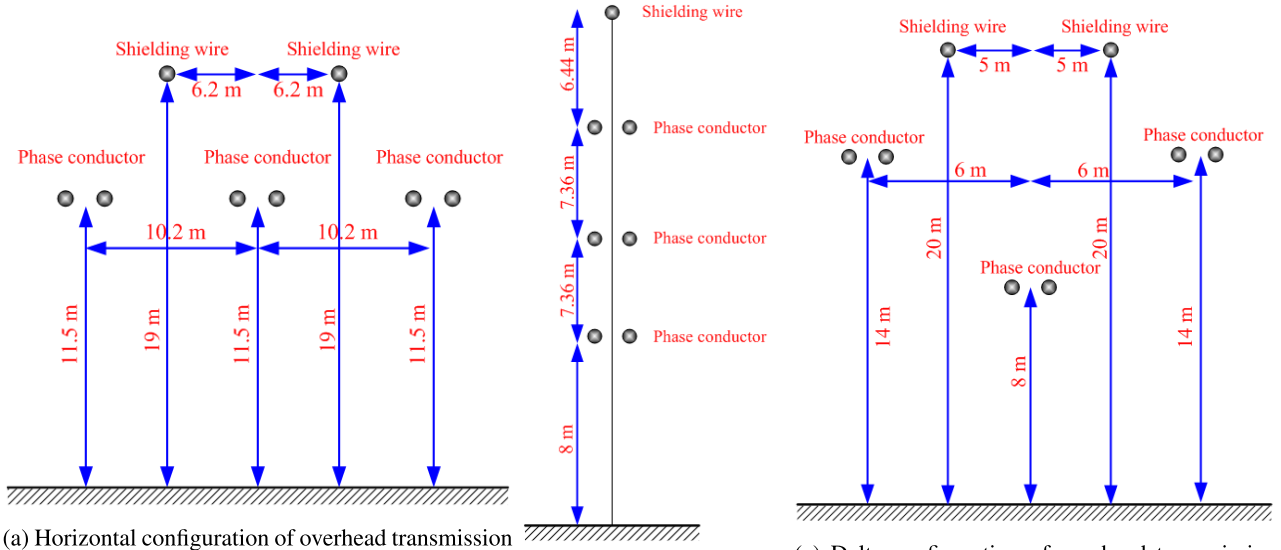

(a) Horizontal configuration of overhead transmission line

(b) Vertical configuration of overhead transmission line

(c) Delta configuration of overhead transmission line

FIGURE 8. **Geometries of the analysed overhead transmission lines used for validation.**

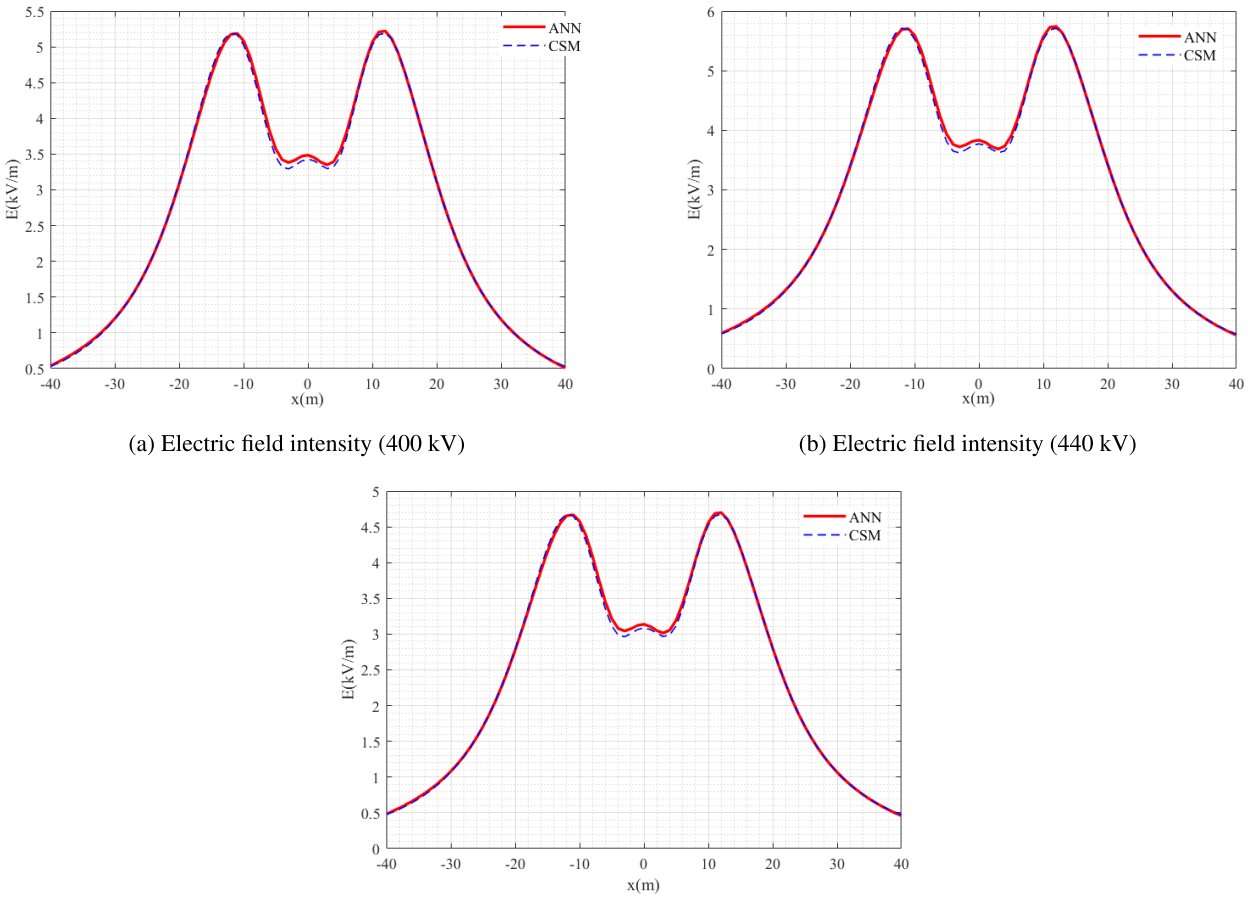

(a) Electric field intensity (400 kV)

(b) Electric field intensity (440 kV)

(c) Electric field intensity (360 kV)

FIGURE 9. **Electric field intensity for the horizontal configuration of phase conductors.**

method and proposed method for the horizontal configuration of phase conductors are shown. Two different applied current values were considered. Figs. 11 and 12 show the results for electric field intensity and magnetic flux density calculation

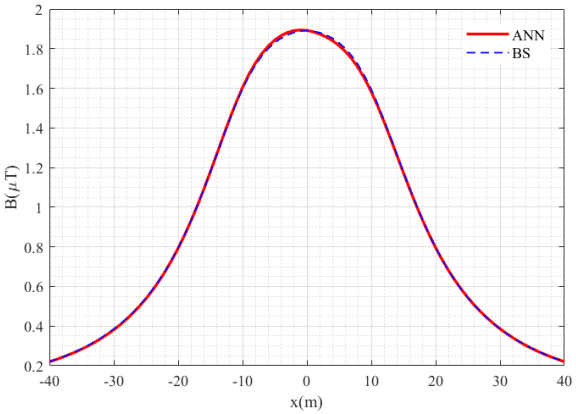

(a) Magnetic flux density (100 A)

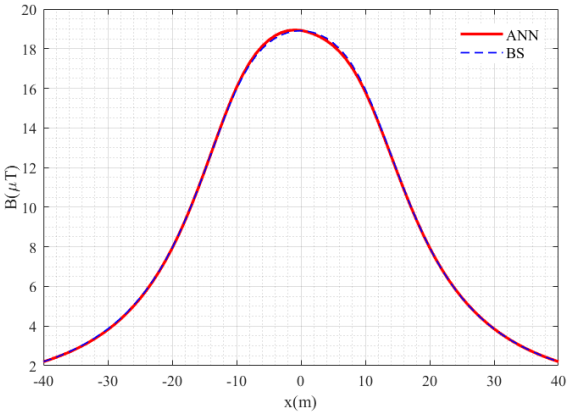

(b) Magnetic flux density (1000 A)

FIGURE 10. Magnetic flux density for the horizontal configuration of phase conductors.

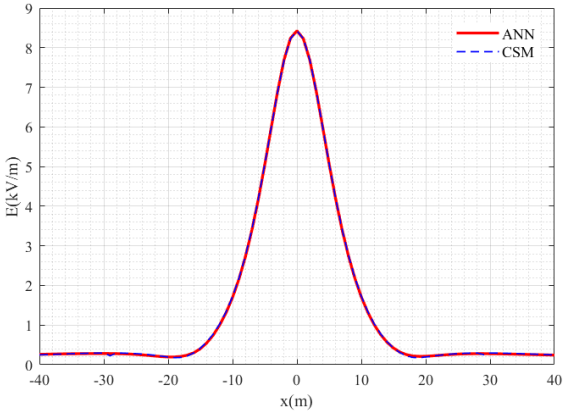

(a) Electric field intensity (400 kV)

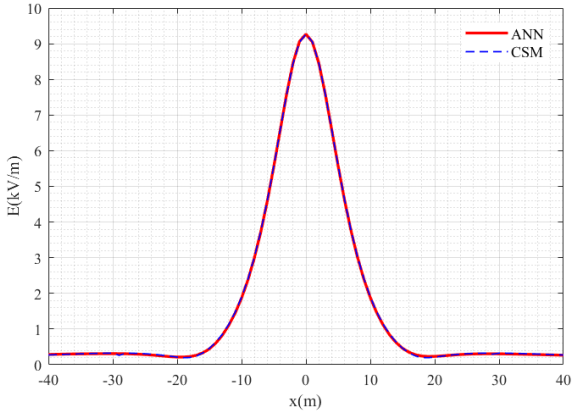

(b) Electric field intensity (440 kV)

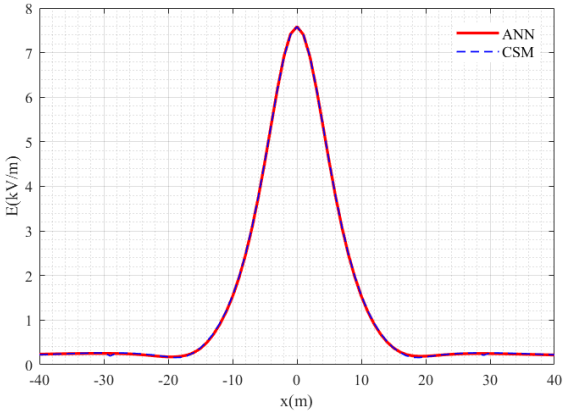

(c) Electric field intensity (360 kV)

FIGURE 11. Electric field intensity for the vertical configuration of phase conductors.

corresponding to the vertical configuration of the overhead transmission line. Figs. 13 and 14 show the results for electric field intensity and magnetic flux density calculations corresponding to the delta phase conductor configuration with two shielding wires.

The results given in Figs 9 - 14 show that the proposed method is able to generate electric field intensity and magnetic flux density results that very closely match the results obtained by CSM and BS law based method for all considered overhead transmission line configurations, applied

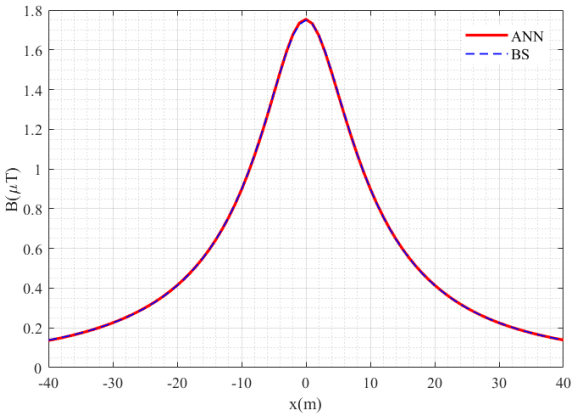

(a) Magnetic flux density (100 A)

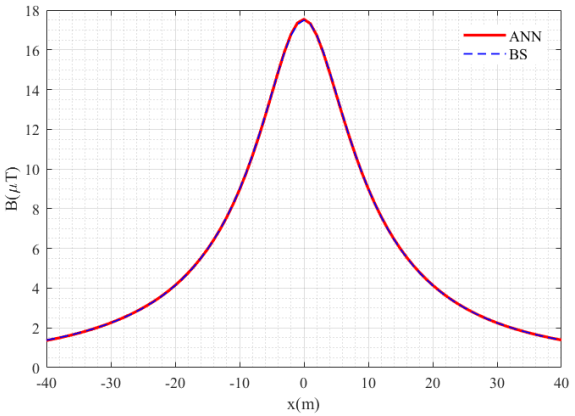

(b) Magnetic flux density (1000 A)

FIGURE 12. Magnetic flux density for the vertical configuration of phase conductors.

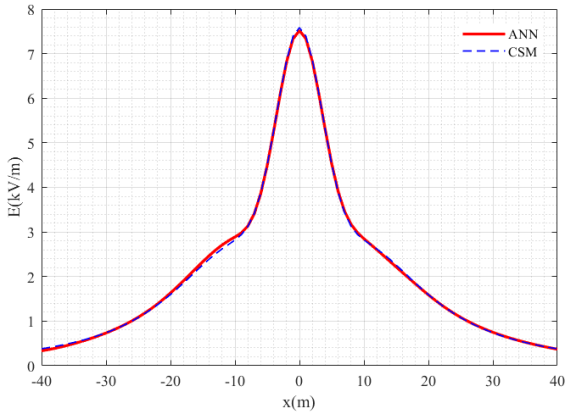

(a) Electric field intensity (400 kV)

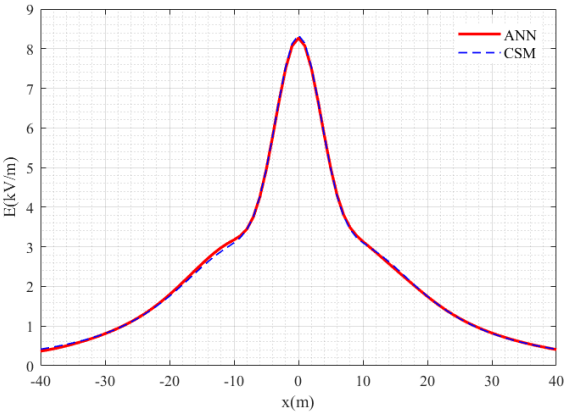

(b) Electric field intensity (440 kV)

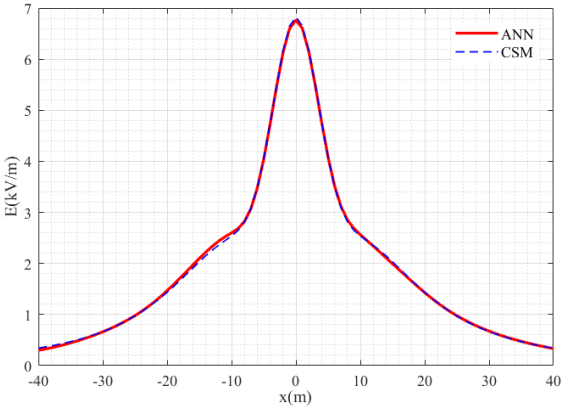

(c) Electric field intensity (360 kV)

FIGURE 13. Electric field intensity for the delta configuration of phase conductors.

voltage and current intensity values over the entire considered lateral profile. The results show that the proposed method can be used to accurately estimate the electric field intensity and magnetic flux density values, irrespective of geometric description of overhead transmission lines. Although ANNs are trained for a fixed applied voltage and current intensity, the results show that the application of the proposed method is clearly not constrained to these particular applied voltage and current intensity values. This property of the proposed method is discussed in previous section.

B. COMPARISON WITH MEASUREMENT RESULTS

The results of the proposed method are also compared with measurement results obtained on two overhead transmission

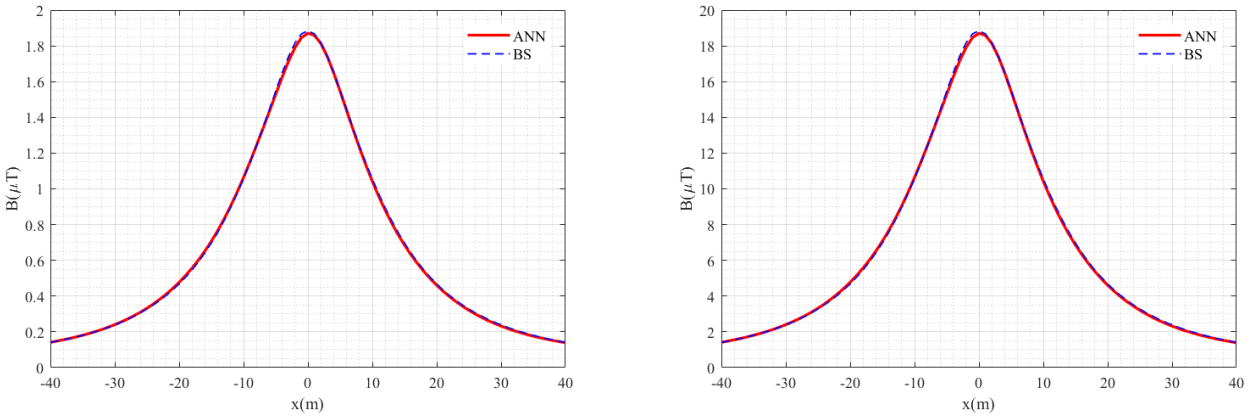

(a) Magnetic flux density (100 A)

(b) Magnetic flux density (1000 A)

FIGURE 14. Magnetic flux density for the delta configuration of phase conductors.

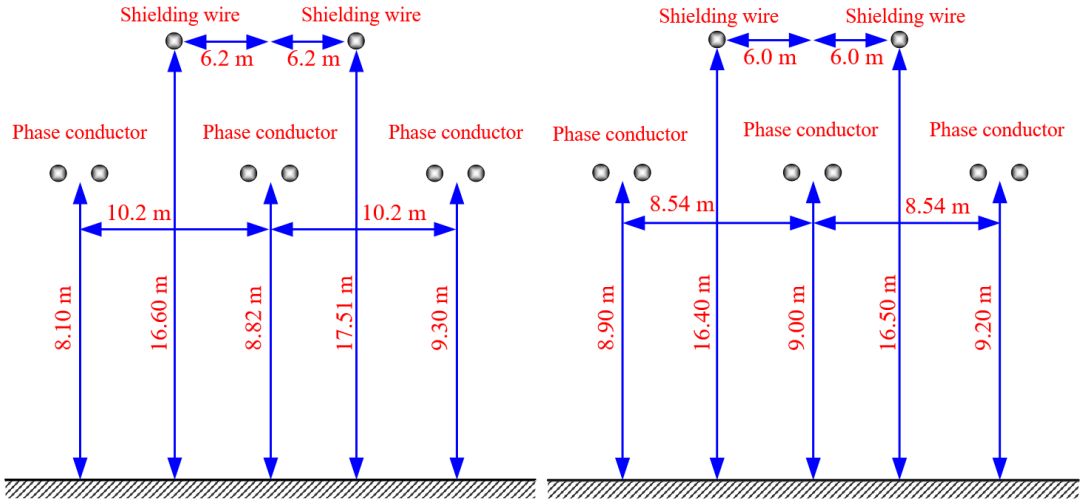

(a) Configuration of overhead transmission line SS Sarajevo 10 - SS Sarajevo 20

(b) Configuration of overhead transmission line SS Tuzla 4 - SS Višegrad

FIGURE 15. Geometries of analysed overhead transmission lines.

lines SS Sarajevo 10 - SS Sarajevo 20 (tower type AKZ Y) and SS Tuzla 4 - SS Višegrad (tower type AKZ YN). Both transmission lines correspond to horizontal phase conductor configurations, first is the standard dimension and the second one is the reduced dimension, as shown in Fig. 15. On both analysed transmission lines, phase conductors are bundle conductors composed of two sub-conductors. For the calculation the values of applied voltage and current intensity are obtained from SCADA system. The height of each conductor has been measured by using height meter Suparule model 600. The electric field intensity measurements have been done by using 1D sensor (HI-3604 ELF Survey Meter) and the magnetic flux density has been measured using the 3D sensor (Narda ELT - 400). Measurement are taken at the height of 1 m above ground surface according to [45]. Lateral profile measurements are performed near the midspan, at minimum conductor height, because highest field values are expected [46].

At the time of measurement of electric field intensity and magnetic flux density, results obtained from SCADA system show that applied voltage was 422.97 kV and that there was no significant variation of the applied voltage over the time of measurement of electric field intensity [47]. On the other hand, during the magnetic flux density measurements the current intensity has had significant variations, as shown in Fig. 16b. For the calculation of magnetic flux density the current intensity of 86.88 A is used as the input parameter.

In Fig. 17, an additional validation of the proposed method with the measurement results is presented, for transmission line given in Fig 15b.

As it can be noted from the results given in Figs. 17a and 17b, both the electric field intensity and the magnetic flux density estimates obtained by the proposed method match very well with the results obtained by CSM and BS law based model. On the other hand, the measurement results slightly deviate from the calculated values. The reason for these

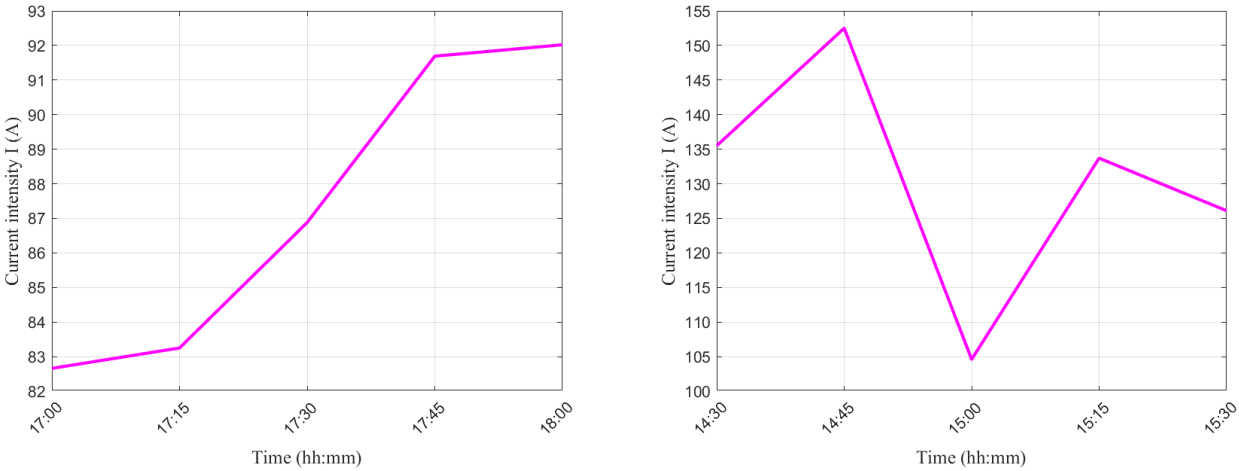

(a) Current on transmission line SS Sarajevo 10 - SS Sarajevo 20

(b) Current on transmission line SS Tuzla 4 - SS Višegrad

FIGURE 16. **Change of transmission line current intensity over the time of measurement.**

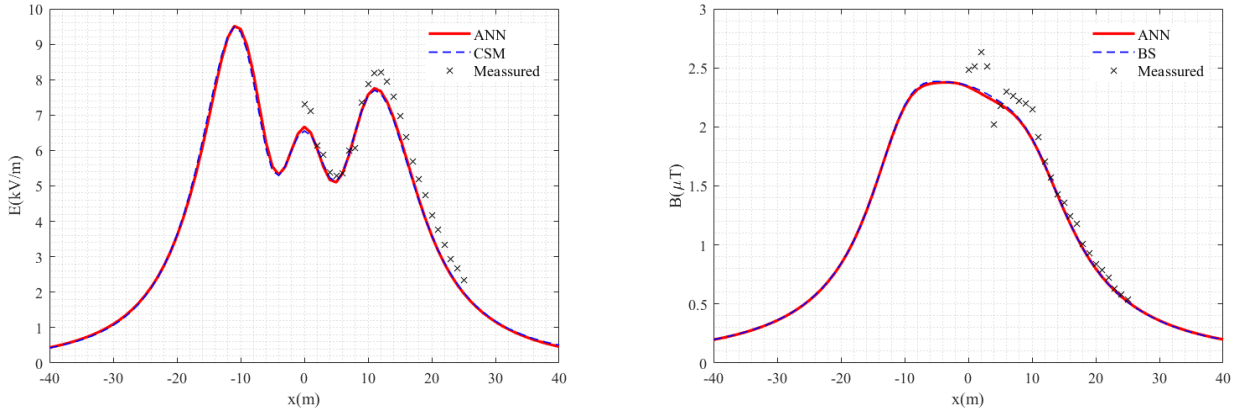

(a) Electric field intensity distribution

(b) Magnetic flux density distribution

FIGURE 17. **Comparison of measured and calculated results under horizontal overhead transmission line of standard dimensions.**

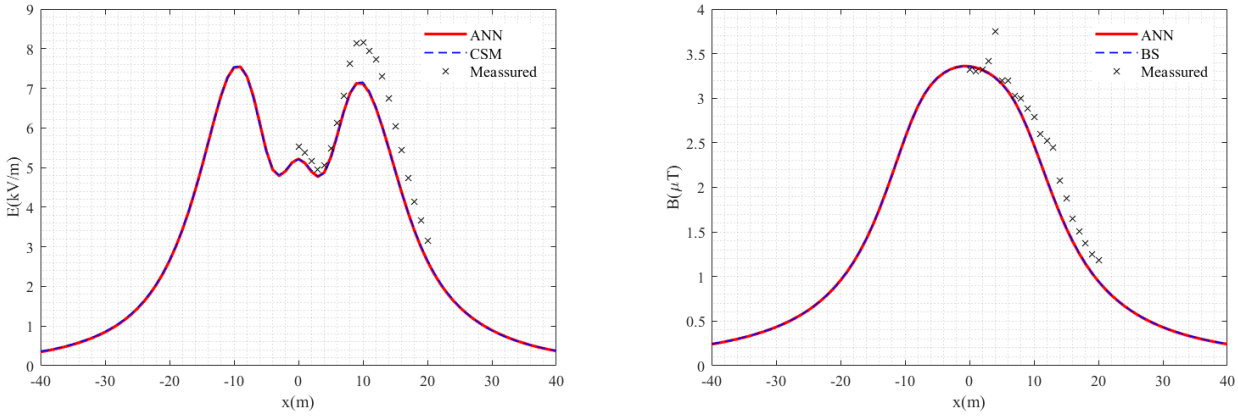

(a) Electric field intensity distribution

(b) Magnetic flux density distribution

FIGURE 18. **Comparison of measured and calculated results under horizontal overhead transmission line of reduced dimensions.**

discrepancies in the electric field intensity are the uneven terrain, operator proximity, and close proximity of shrubs to measurement location. The reason for the observed discrepancies in the magnetic flux density are current intensity variation during magnetic flux density measurements and unsymmetrical current flow on phase conductors.

Second case analysed within this section is overhead transmission line of horizontal configuration with reduced dimension, given in Fig. 15b.

At the time of electric field intensity and magnetic flux density measurements, results obtained from SCADA system show that applied voltage was 416 kV and there was no significant variation of the applied voltage over the time of measurement of electric field intensity [47]. On the other hand, during the time of magnetic flux density measurements the current intensity had significant variation, as shown in Fig. 16b. For the calculation of magnetic flux density, the current intensity of 133.16 A is used as an input parameter.

In Figs. 18a and 18b additional validation of the proposed method with measurement results is presented.

Similarly, as in previously discussed case, the proposed method produces electric filed intensity and magnetic flux density estimates that closely match the calculation results obtained via CSM and BS law based method, respectively. As expected, there are slight discrepancies between the results of the proposed method and the measurement data due to the previously discussed reasons.

IV. CONCLUSION

In the process of planning of new overhead transmission lines, it is important to accurately calculate the maximum levels of electric and magnetic fields that may occur in the proximity of transmission lines in order to meet the allowed values. In this paper, a novel method for electric field intensity and magnetic flux density estimation in the vicinity of the high voltage overhead transmission lines is proposed. The proposed method is based on two fully connected feed-forward neural networks models, where one ANN model is used for electric field intensity estimation, while the second ANN model is used for magnetic flux density estimation. Artificial neural network is a massively parallel distributed processor, which has an inherent predisposition for learning and generalization. Fully connected feed-forward neural networks have the capacity to represent complex nonlinear input output relations. The ANN training dataset is generated using different overhead transmission line configurations. Different overhead transmission line configurations are generated using an algorithm that is especially developed for this purpose. The target values for the electric field intensity and magnetic flux density datasets are evaluated using the CSM and BS law based method, respectively. The scaled conjugate gradient algorithm is used to train the ANNs. The experimental results show that the proposed method is able to accurately estimate electric field intensity and magnetic flux density values that very closely match the results obtained by CSM and BS law method for all considered overhead transmission line configurations, applied voltage and current intensity values, over the entire considered lateral profile. Due to the aforementioned characteristics of the proposed method, the proposed method could be successfully applied into high voltage transmission line design optimization. In addition, the proposed method is evaluated on electric field intensity and magnetic flux density measurement results obtained on two overhead transmission lines SS Sarajevo 10 - SS Sarajevo 20 and SS Tuzla 4 - SS Višegrad.

REFERENCES

[1] A. Amoon, C. Crespi, A. Ahlbom, M. Bhatnagar, I. Bray, K. Bunch, J. Clavel, M. Feychting, D. Hémon, C. Johansen, C. Kreis, C. Malagoli, F. Marquant, C. Pedersen, O. Raaschou-Nielsen, M. Röösli, and B. Spycher, "Proximity to overhead power lines and childhood leukaemia: An international pooled analysis," *Brit. J. Cancer*, vol. 119, no. 3, pp. 364–373, Aug. 2018.

[2] C. Sermage-Faure, C. Demoury, J. Rudant, S. Goujon-Bellec, A. Guyot-Goubin, F. Deschamps, D. Hemon, and J. Clavel, "Childhood leukaemia close to high-voltage power lines–the Geocap study, 2002–2007," *Brit. J. cancer*, vol. 108, no. 9, pp. 1899–1906, 2013.

[3] C. M. Crespi, X. P. Vergara, C. Hooper, S. Oksuzyan, S. Wu, M. Cockburn, and L. Kheifets, "Childhood leukaemia and distance from power lines in California: A population-based case-control study," *Brit. J. Cancer*, vol. 115, no. 1, pp. 122–128, Jun. 2016.

[4] M. Gallastegi, A. Jiménez-Zabala, L. Santa-Marina, J. J. Aurrekoetxea, M. Ayerdi, J. Ibarluzea, H. Kromhout, J. González, and A. Huss, "Exposure to extremely low and intermediate-frequency magnetic and electric fields among children from the INMA-Gipuzkoa cohort," *Environ. Res.*, vol. 157, pp. 190–197, Aug. 2017.

[5] E. Lunca, S. Ursache, and A. Salceanu, "Computation and analysis of the extremely low frequency electric and magnetic fields generated by two designs of 400 kV overhead transmission lines," *Measurement*, vol. 124, pp. 197–204, Aug. 2018.

[6] T. Samaras, N. Leitgeb, A. Auvinen, H. Danker-Hopfe, K. H. Mild, M.-O. Mattsson, H. Norppa, G. Rubin, M. R. Scarfi, J. Schüz, Z. Sienkiewicz, and O. Zeni, "Scientific committee on emerging and newly identified health risks), potential health effects of exposure to electromagnetic fields (EMF)," Eur. Commission, Brussels, Belgium, Tech. Rep., Jan. 2015.

[7] J. Lin, R. Saunders, K. Schulmeister, P. Söderberg, B. Stuck, A. Swerdlow, M. Taki, B. Veyret, G. Ziegelberger, M. Repacholi, R. Matthes, A. Ahlbom, K. Jokela, and C. Roy, "ICNIRP guidelines for limiting exposure to time-varying electric and magnetic fields (1 Hz to 100 kHz)," *Health Phys.*, vol. 99, no. 6, pp. 818–836, 2010.

[8] D. Poljak, "Exposure to non-ionising electromagnetic fields from extremely low to microwave frequencies," *Arch. Ind. Hygiene Toxicol.*, vol. 61, 2010.

[9] J. S. Acosta and M. C. Tavares, "Optimal selection and positioning of conductors in multi-circuit overhead transmission lines using evolutionary computing," *Electr. Power Syst. Res.*, vol. 180, Mar. 2020, Art. no. 106174.

[10] I. A. M. Duane, M. M. Afonso, M. A. D. O. Schroeder, S. T. M. Gonçalves, A. L. Paganotti, and R. R. Saldanha, "A new strategy for optimizing HSIL transmission lines," *J. Control, Autom. Electr. Syst.*, vol. 31, no. 5, pp. 1288–1297, Oct. 2020.

[11] J. S. Acosta and M. C. Tavares, "Methodology for optimizing the capacity and costs of overhead transmission lines by modifying their bundle geometry," *Electr. Power Syst. Res.*, vol. 163, pp. 668–677, Oct. 2018.

[12] K. Król and W. Machczynski, "Optimization of electric field intensity under power transmission line with use of genetic algorithm and particle swarm algorithms," *Arch. Electr. Eng.*, vol. 67, no. 4, pp. 1–15, 2018.

[13] F. Muñoz, J. A. Aguado, F. Martín, J. J. López, A. Rodríguez, J. B. García, A. R. Treitero, and R. Molina, "An intelligent computing technique to estimate the magnetic field generated by overhead transmission lines using a hybrid GA-Sx algorithm," *Int. J. Electr. Power Energy Syst.*, vol. 53, pp. 43–53, Dec. 2013.

[14] V. Ranković and J. Radulović, "Prediction of magnetic field near power lines by normalized radial basis function network," *Adv. Eng. Softw.*, vol. 42, no. 11, pp. 934–938, Nov. 2011.

[15] A. E. Tzinevrakis, D. K. Tsanakas, and E. I. Mimos, "Electric field analytical formulas for single-circuit power lines with a horizontal arrangement of conductors," *IET Gener., Transmiss. Distrib.*, vol. 3, no. 6, pp. 509–520, Jun. 2009.

[16] W. T. Kaune and L. E. Zaffanella, "Analysis of magnetic fields produced far from electric power lines," *IEEE Trans. Power Del.*, vol. 7, no. 4, pp. 2082–2091, Oct. 1992.

[17] A. Geri, A. Locatelli, and G. M. Veca, "Magnetic fields generated by power lines," *IEEE Trans. Magn.*, vol. 31, no. 3, pp. 1508–1511, May 1995.

[18] T. Modrić, S. Vujević, and D. Lovrić, "A surface charge simulation method based on advanced numerical integration," *Adv. Eng. Softw.*, vol. 86, pp. 20–28, Aug. 2015.
[19] D. Rabah, C. Abdelghani, and H. Abdelchafik, "Efficiency of some optimisation approaches with the charge simulation method for calculating the electric field under extra high voltage power lines," *IET Gener., Transmiss. Distrib.*, vol. 11, no. 17, pp. 4167–4174, Nov. 2017.
[20] R. Wang, J. Tian, F. Wu, Z. Zhang, and H. Liu, "PSO/GA combined with charge simulation method for the electric field under transmission lines in 3D calculation model," *Electronics*, vol. 8, no. 10, p. 1140, Oct. 2019.
[21] C. A. Belhadj and S. El-Ferik, "Electric and magnetic fields estimation for live transmission line right of way workers using artificial neural network," in *Proc. 15th Int. Conf. Intell. Syst. Appl. Power Syst.*, Nov. 2009, pp. 1–6.
[22] H. F. Carlak, Ş. Özen, and S. Bilgin, "Low-frequency exposure analysis using electric and magnetic field measurements and predictions in the proximity of power transmission lines in urban areas," *Turkish J. Electr. Eng. Comput. Sci.*, vol. 25, no. 5, pp. 3994–4005, 2017.
[23] S. Haykin, *Neural Networks and Learning Machines*, 3rd ed. London, U.K.: Pearson, 2009.
[24] J. Fan, L. Fang, J. Wu, Y. Guo, and Q. Dai, "From brain science to artificial intelligence," *Engineering*, vol. 6, no. 3, pp. 248–252, Mar. 2020.
[25] Z. Zhao, Z. Wang, J. Yuan, J. Ma, Z. He, Y. Xu, X. Shen, and L. Zhu, "Development of a novel feedforward neural network model based on controllable parameters for predicting effluent total nitrogen," *Engineering*, vol. 7, no. 2, pp. 195–202, Feb. 2021.
[26] X. Qi, G. Chen, Y. Li, X. Cheng, and C. Li, "Applying neural-network-based machine learning to additive manufacturing: Current applications, challenges, and future perspectives," *Engineering*, vol. 5, no. 4, pp. 721–729, Aug. 2019.
[27] M. Møller, "A scaled conjugate gradient algorithm for fast supervised learning," *Neural Netw.*, vol. 6, no. 4, pp. 525–533, 1993.
[28] W. W. Hager and H. Zhang, "A survey of nonlinear conjugate gradient methods," *Pacific J. Optim.*, vol. 2, no. 1, pp. 35–58, Jan. 2006.
[29] M. R. Hestenes and E. Stiefel, "Methods of conjugate gradients for solving linear systems," *J. Res. Nat. Bur. Standards*, vol. 49, pp. 409–435, Dec. 1952.
[30] R. Fletcher and C. M. Reeves, "Function minimization by conjugate gradients," *Comput. J.*, vol. 7, no. 2, pp. 149–154, 1964.
[31] T. Modric, S. Vujević, and D. Lovric, "3D computation of the power lines magnetic field," *Prog. Electromagn. Res.*, vol. 41, pp. 1–9, Jan. 2015.
[32] S. Vujevic and T. Modric, "The influence of conductive passive parts on the magnetic flux density produced by overhead power lines," *Facta Universitatis, Electron. Energetics*, vol. 32, no. 4, pp. 555–569, 2019.
[33] *IEEE Guide for Improving the Lightning Performance of Transmission Lines*, Standard 1243-1997, IEEE, 1997, pp. 1–44.
[34] A. Mujezinović, A. Čarsimamovic, S. Čarsimamovic, A. Muharemovic, and I. Turković, "Electric field calculation around of overhead transmission lines in Bosnia and Herzegovina," in *Proc. Int. Symp. Electromagn. Compat.*, Sep. 2014, pp. 1001–1006.
[35] A. Z. El Dein, M. A. A. Wahab, M. M. Hamada, and T. H. Emmary, "The effects of the span configurations and conductor sag on the electric-field distribution under overhead transmission lines," *IEEE Trans. Power Del.*, vol. 25, no. 4, pp. 2891–2902, Oct. 2010.
[36] T. Modric, S. Vujević, and I. Paladin, "3D computation of the overhead power lines electric field," *Prog. Electromagn. Res. M*, vol. 53, pp. 17–28, Jan. 2017.
[37] J. A. B. Faria and M. E. Almeida, "Accurate calculation of magnetic-field intensity due to overhead power lines with or without mitigation loops with or without capacitor compensation," *IEEE Trans. Power Del.*, vol. 22, no. 2, pp. 951–959, Apr. 2007.
[38] J. Salari, A. Mpalantinos, and J. Silva, "Comparative analysis of 2- and 3-D methods for computing electric and magnetic fields generated by overhead transmission lines," *IEEE Trans. Power Del.*, vol. 24, no. 1, pp. 338–344, May 2009.
[39] A. Z. El Dein, "Parameters affecting the charge distribution along overhead transmission lines' conductors and their resulting electric field," *Electr. Power Syst. Res.*, vol. 108, pp. 198–210, Mar. 2014.
[40] T. Modrić and S. Vujević, "Computation of the electric field in the vicinity of overhead power line towers," *Electr. Power Syst. Res.*, vol. 135, pp. 68–76, Jun. 2016.
[41] *Independent System Operator in Bosnia and Herzegovina*, Grid Code, Sarajevo, Bosnia and Herzegovina, 2019.
[42] *IEC Standard Voltages*, Standard IEC 60038:2009, International Electrotechnical Commission, 2009.
[43] A. Carsimamovic, A. Mujezinovic, Z. Bajramovic, I. Turkovic, M. Kosarac, and K. Stankovic, "Origin and mitigation of increased electric fields at high voltage transmission line conductors," *Int. J. Electr. Power Energy Syst.*, vol. 104, pp. 134–149, Jan. 2019.
[44] S. Carsimamovic, Z. Bajramovic, M. Veledar, M. Ljevak, S. Nuic, and P. Osmokrovic, "Impact of tower dimensions onto levels of elf electric and magnetic fields of 400 kv overhead lines," in *Proc. 32nd Conf. CIGRE*, Paris, France, 2008, pp. 1–7.
[45] *Measurement of DC Magnetic, AC Magnetic and AC Electric Fields From 1 Hz to 100 kHz With Regard to Exposure of Human Beings—Part 2: Basic Standard for Measurements*, *Int. Electrotechnical Commission*, Standard IEC 61786-2:2014, 2014.
[46] *IEEE Standard Procedures for Measurement of Power Frequency Electric and Magnetic Fields From AC Power Lines*, Standard 644-2019, IEEE, 2020, pp. 1–40.
[47] A. Carsimamovic, A. Mujezinovic, Z. Bajramovic, I. Turkovic, and M. Kosarac, "Low frequency electric field radiation level around high-voltage transmission lines and impact of increased voltage values on the corona onset voltage gradient," *Nucl. Technol. Radiat. Protection*, vol. 33, no. 2, pp. 201–207, 2018.

AJDIN ALIHODZIC (Member, IEEE) received the B.S. and M.S. degrees (Hons.) from the Department for Electric Power Engineering, Faculty of Electrical Engineering, University of Sarajevo, in 2015 and 2017, respectively, where he is currently pursuing the Ph.D. degree. From 2017 to 2020, he was an Investment Associate Engineer in the Executive Directorate for Investments at Joint Stock Company BH Telecom. Since 2020, he has been a Teaching Assistant/a Research Assistant with the University of Sarajevo. His research interests include numerical techniques in electromagnetics, transmission lines, and artificial intelligence.

ADNAN MUJEZINOVIC (Member, IEEE) received the M.Sc. and Ph.D. degrees in electrical engineering from the Faculty of Electrical Engineering, University of Sarajevo, Bosnia and Herzegovina, in 2011 and 2017, respectively. Since 2012, he has been with the Faculty of Electrical Engineering, University of Sarajevo, as a Teaching Assistant, and currently, as an Assistant Professor. He has authored numerous conference papers and journal articles. His research interests include numerical calculations of electromagnetic fields, cathodic protection, and transmission lines.

EMIR TURAJLIC (Member, IEEE) received the Ph.D. degree from Brunel University London, U.K., in 2007. He is currently an Associate Professor with the Department of Telecommunications, Faculty of Electrical Engineering, University of Sarajevo, Bosnia and Herzegovina. He has authored numerous conference papers and journal articles. He has written books on artificial neural networks, and image and video compression. His primary research interests include the fields of digital signal processing, speech processing, artificial intelligence, and machine learning. He has expanded his research to include image processing, data compression, and metaheuristic algorithms.